RESERVE THIS SPACE

Model Polymer Thin Films to Measure Structure & Dynamics of Confined, Swollen Networks

Sara V. Orski, Kirt A. Page, Edwin P. Chan,* Kathryn L. Beers*

Materials Science and Engineering Division, The National Institute of Standards and Technology (NIST), Gaithersburg, MD 20899 USA

* kathryn.beers@nist.gov and edwin.chan@nist.gov

Abstract

In this chapter, we discuss applying X-ray reflectivity to study the structure and dynamics of dense and ultrathin polymer films upon exposure to solvent vapors. These vapor swelling studies permit the measurement of thermodynamic parameters using established mean-field models such as Flory-Huggins, Flory-Rehner, and Painter-Shenoy to understand the elastic contributions to swelling, as well as the polymer solvent interaction parameter of these confined films. This chapter describes the various experimental approaches to leverage mean-field theories towards describing and understanding swelling behavior of thin film networks and brushes, the applications, and their limitations.

RESERVE THIS SPACE

Introduction

Polymer thin films over the last several decades have advanced beyond conventional, passive coatings and filters to active semi-permeable membranes that have a delicate interplay between analytes, the solvent or gas environment, the thin film support surface, and neighboring polymer chains. Thin film membranes have developed a broad application space, from acting as environmental absorbents or biological scaffolds, to controlling fouling or separating large and small molecules in the liquid or gas phase.[1–5] Development of these advanced polymer thin film membranes have been largely empirical as material optimization is generally tailored to improving performance, such as selectivity of one analyte over a small list of competing species, for practical and commercial uses. Fundamental metrology of membrane molecular structure, chain morphology, thermodynamics and (ultimately) correlation to performance of these materials have also been limited, especially for *in situ* measurements, as films are often sub-100 nm in thickness, which limit the tools available to measure these parameters. The design of next-generation films requires accurate structure/property relationships and a fundamental understanding of critical structural and thermodynamic parameters that affect performance such as analyte diffusivity, solubility, pore size, pore size distributions, stability, and service life.

Using two case studies – polymer membranes for water purification and grafted polymer brushes for tailored surface chromatography separation methods – we demonstrate major advances in metrology designed to support basic research into characterization of ultra-thin polymer networks.[6–8] This chapter covers recent advances in the synergistic approach to understanding swelling behavior in these films by combining synthetic design of controlled, homogeneous model thin films, with X-ray reflectivity measurements to measure changes in film thickness, roughness, and material density when exposed to solvent vapor. These changes upon swelling can be applied to mean field thermodynamic models to understand when the enthalpic and entropic contributions to swelling agree with established theoretical models or when new models need to be developed to account for additional parameters that may not be incorporated into existing theories.

X-ray Reflectivity to Study Thin Film Structure

Overview

Swelling is a classic approach used to interrogate the structure of a crosslinked polymer network. This approach measures the amount of solvent uptake as a function of solvent activity and then applies the appropriate equation-of-state to determine the thermodynamic parameters of the polymer network. Swelling measurements are straightforward for macroscopic specimens since it simply relates swelling to solvent activity by measuring the change in specimen mass or specimen dimensions. Measuring the swelling behavior is non-trivial for ultrathin films because of the diminishingly small changes in mass and volume due to solvent uptake, as well as adsorption that can occur at the interface between the ultrathin film and its supporting layer.[9–11]

This chapter describes the application of specular X-ray reflectivity (XR) to measure the dimensional change of polymer thin film networks due to vapor swelling. XR is a high-resolution measurement technique for studying the interfaces of materials possessing different electron densities with resolution of approximately 0.1 nm.[12,13] XR has been widely used to study soft materials such as photoresists,[14] polymer glasses,[15–17] nanoimprinted polymers,[18,19] polymer bilayers,[20] polymer brushes,[21] gel layers[22,23], polyelectrolyte multilayers[24,25] and membrane layers[26] over the past two decades. XR is particularly suited for conducting polymer thin films thermodynamic studies, as repeated measurements of a specimen area can be conducted, limiting uncertainty due to batch to batch variation of thin film samples.

Vapor Swelling of Polymer Thin Films

A typical XR measurement of a polymer thin film is illustrated in Figure 1a. An X-ray beam is directed onto the polymer film that is supported by a substrate in a vacuum or air environment. Typically, the incident X-ray is directed at a glancing angle from ≈0.1° to 1° and then the scattered beam is measured at the specular condition, *i.e.* where the incident angle equals the reflected angle. Several properties of the substrate-supported polymer film can be quantified with an X-ray reflectivity measurement. These properties include the thickness (h), the roughness (σ), and the electron density (Q_c^2). For more complex films such as polymer multilayers, XR can also quantify the thickness, roughness and density for each layer if there is sufficient electron contrast between layers and they are sufficiently smooth. The reflectivity curve is typically presented as a plot of reflectivity (R(Q)) versus the incident angle (θ) or the scattering vector (Q). Below

the critical angle or the critical scattering vector (Q_c), R(Q) remains constant at the maximum value, as the incident irradiation is completely reflected. Above Q_c, when the incident radiation penetrates into the film thus resulting in scattering at the various interfaces, oscillations or interference fringes occur. As a result, R(Q) drops abruptly and decays with increasing Q. Film thickness is determined by successive minima or maxima (ΔQ) of the fringes, which is equivalent to $2\pi/h$. Real material interfaces are not infinitely sharp and display a gradient in density from the surface into the bulk of the material. We will not go into detail about the effects of roughness on reflectivity as many others have already discussed this topic.[13,27]

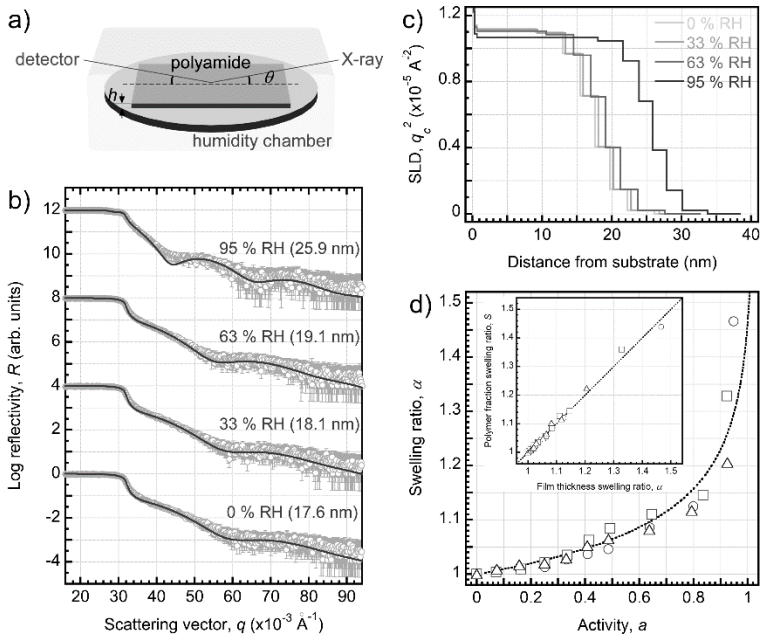

Figure 1. *Studying the swelling behavior of commercial PA NF membrane selective layer via XR. a) Sample geometry of XR. b) Reflectivity versus scattering vector curves as a function of relative humidity illustrating the PA layer expansion. The solid black curves are the best fits of the reflectivity data. c) Electron density change as a function of relative humidity. d) Thickness swelling ratio as a function of water activity measured using 3 separate PA samples. The curve is a fit to the data as defined by the Flory-Rehner theory for one-dimensional swelling.* [28] *The inset figure shows the linear relationship between thickness change and mass change, thus indicating that the selective layer swells only along the thickness direction. Reproduced with permission from reference 28. Copyright 2013 John Wiley & Sons.*

All XR measurements described in this chapter were performed using a Phillips X'PERT X-ray diffractometer with a Cu K_α source (λ=0.154 nm. The X-ray beam was focused using a curved mirror into a quadruple bounce Ge [220] crystal monochromator. The specular condition was obtained for the reflected beam using a triple bounce Ge [220] crystal monochromator. The scattering vector was calculated from:

$$Q = \frac{4\pi \sin\theta}{\lambda} \quad (1)$$

where θ is the incident angle and λ is the wavelength of the X-ray beam. Specular reflectivity curves were collected from 0.1° up to a maximum angle of 1.5° for each film, depending on the largest angle where additional fringes were not discernable due to surface roughness.

Vapor swelling experiments were performed at 25 °C using an aluminum chamber sealed over the target substrate with X-ray transparent beryllium windows. A dual mass flow controller system to control vapor mixing and thus vary the partial pressure of solvent was assembled according to literature procedures.[29] All films were allowed to equilibrate at each activity until reflectivity curves were identical between successive scans. This protocol was used to ensure the chamber was temperature equilibrated at each vapor concentration before measurement. Calibration of the actual activity within the chamber relative to the mass flow controller settings was performed by using either a humidity sensor for water vapor, or by flowing the vapor through a quartz cell in a UV-vis spectrometer and using the integrated absorption area of the solvent peak normalized to the area measuring from the saturated vapor attained using a solvent reservoir, in the case of organic vapors. For the highest solvent activities measured ($a_s \geq 0.95$), an open reservoir of solvent was allowed to equilibrate in the closed chamber until vapor saturation was reached.

Data reduction for each reflectivity curve was performed using a MATLAB routine that consisted of footprint correction and conversion of the scattering angle into scattering vector. Theoretical reflectivity curves were modeled using NIST Reflfit software,[30] which uses Parratt's formalism for given layer thickness and scattering length densities. Fitting the model to experimental data yielded film thickness, scattering length density, roughness, and linear absorption coefficient; the quality of fit was indicated by Pearson's chi-squared test. Initial predictions of Q_c^2 for each solvent, polymer thin film, and bulk silicon were calculated from the NIST NCNR website.[31]

Determination of Thin Film Swelling Ratios and Dimensionality

The thickness information about each layer obtained from the reflectivity curves at each solvent activity (a_s) can be used to determine the thickness swelling

ratio, α, The thickness swelling ratio at each activity was calculated using equation 2:

$$\alpha = \frac{h_s}{h_d} \tag{2}$$

where h_d and h_s are the film thickness in the dry and swollen state. Evaluating the thickness increase alone is insufficient in understanding the complete swelling behavior of the layer since lateral expansion of the layer cannot be determined. The volumetric swelling of the selective layer is determined by comparing the change in the measured Q_c^2 at a given a_s ($Q_c^2{}_x$) with known or measured Q_c^2 in the dry film ($Q_c^2{}_{dry}$) and the solvent ($Q_c^2{}_{solvent}$). Since the electron density is directly related to the mass density, this parameter can be used to estimate the volume fraction of the polymer (ϕ_p) relative to the solvent volume fraction (ϕ_s) in the swollen layer by:

$$\phi_p = \frac{Q_c^2{}_x - Q_c^2{}_{solvent}}{Q_c^2{}_{dry} - Q_c^2{}_{solvent}} \tag{3}$$

$$\phi_s = 1 - \phi_p \tag{4}$$

The polymer volume fraction was then converted to a volume fraction swelling ratio (S) and compared with the thickness swelling ratio,

$$S = \frac{1}{\phi_p};\ \ \phi_p = \frac{1}{\alpha^n};\log S = n\log\alpha \tag{5a, 5b, 5c}$$

Swelling dimensionality (n) is needed to derive proper theromdynamic models based on whether the chains swell isotropically (n=3) or unidirectionally (n=1). All experiments in this chapter have displayed 1D swelling based on dimensionality calculations. It is important to note that while the polymer volume fraction can be used to calculate the volumetric swelling of the PA, the uncertainty of Qc^2 is significantly greater than h, meaning that α should be used over ϕ whenever swelling dimensionality is consistent across all measured activities. Another issue is that calculating the polymer volume fraction requires a density difference between the polymer and the solvent, which is not always possible.

Thermodynamic Models

Once swelling ratios and the corresponding dimensionality of the swollen polymer thin film have been established, mean field models can be applied to characterize swelling thermodynamic parameters in the polymer thin film networks. Solvent uptake with systematic change of the chemical potential are described by equations 6 and 7, beginning with conventional Flory-Huggins[32] theory ($(\delta\Delta G/\delta n_s)_{el} = 0$) as well as adaptations for entropic, elastic contributions to the chemical potential change in the networks ($(\delta\Delta G/\delta n_s)_{el}$) via Flory-Rehner[33]

and Painter-Shenoy[34] models. The Flory-Rehner and Painter-Shenoy models share two fundamental assumptions about the thermodynamics of the system, 1) that the free energy of swelling can be separated into distinct contributions from mixing and elastic energies (equation 6) and 2) that the mixing contribution to the energy (and therefore chemical potential) change upon swelling of the network follows Flory-Huggins theory of mixing.

$$\Delta\mu_s = \frac{\partial}{\partial n_s}\Delta G_{total} = \frac{\partial}{\partial n_s}(\Delta G_{mix} + \Delta G_{el}) \quad (6)$$

$$\frac{\partial \Delta G_{mix}}{\partial n_s} = RT\, ln(a_s) = RT\left[\ln\left(1-\phi_p\right) + \phi_p + \chi\phi_p{}^2\right] \quad (7)$$

Flory-Rehner and Painter-Shenoy models differ in their final assumption of the system. Flory Rehner makes the assumption that swelling is affine, which implies that the solvent distribution within the network is homogeneous.[28,35,36] The elastic contribution to the free energy change for 1D swelling for the Flory-Rehner model has been derived[28] and is shown in equation 8, where N is the number of monomer units between crosslinks. Substituting equation 8 into equation 2 yields the full chemical potential change of the swollen network and is shown in the full Flory-Rehner equation (equation 9).

$$\left(\frac{1}{RT}\right)\frac{\partial \Delta G_{el}}{\partial n_s} = \frac{1}{N_s} * \left(\frac{1}{\phi} - \frac{\phi}{2}\right) \quad (8)$$

$$\Delta\mu_s = RT\left[\ln\left(1-\phi_p\right) + \phi_p + \chi\phi_p{}^2 + \frac{1}{N_s} * \left(\frac{1}{\phi} - \frac{\phi}{2}\right)\right] \quad (9)$$

Since the chemical potential was derived in terms of the change in the number of solvent molecules, N must be in terms of the solvent molar volume equilvent, which is denoted as N_s.

In the Painter-Shenoy model, the swelling of the network is not affine and consists of polymer chain expansion with topological rearrangement of the network junctions, which results in heterogeneous solvent distribution where there are solvent-rich regions devoid of polymer chains. The degree of cross-linking can affect the χ parameter as well,[37] as different mechanisms to make a cross-linked thin film can result in different molecular masses between crosslinks that can interact with different amounts of absorbing solvent, yielding different solvated properties.[38] The elastic contribution to the free energy change for Painter-Shenoy 1D swelling has been derived and is shown in equation 10, where f is the functionality of the network junctions, or the number of chains tethered at a single crosslink location in the network. The full Painter-Shenoy expression for the chemical potential change is shown in equation 11.

$$\left(\frac{1}{RT}\right)\frac{\partial \Delta G_{el}}{\partial n_s} = \frac{1}{N_s{}^2\phi_p} * \left(\frac{1}{2} - \frac{2}{f}\right)\left(\frac{\phi_p}{N_s}\right) \quad (10)$$

$$\Delta\mu_s = RT\left[\ln\left(1-\phi_p\right)+\phi_p+\chi{\phi_p}^2+\frac{1}{{N_s}^2\phi_p}*\left(\frac{1}{2}-\frac{2}{f}\right)\left(\frac{\phi_p}{N_s}\right)\right] \quad (11)$$

One must take great care in choosing a thermodynamic model with which to analyze the reflectivity data. It is important that the model has a physical basis and that the scattering model is consistent with a real-space image obtained from microscopy. While scattering techniques have been used for the last two decades to study these materials, there remain many challenges and opportunities to develop comprehensive models and techniques to elucidate the structure-property-performance relationships in these functional materials.

Model Polyamide Networks for Water Desalination

XR has been used to understand the structure of water desalination membranes. Water desalination, based on pressure-driven membrane separations such as reverse osmosis (RO) or nanofiltration (NF), is currently the most widely used commercial technology for providing clean and sustainable water supplies,[39] as they are considered the most energy efficient and high-throughput technologies over methods such as distillation and forward osmosis.

An ideal desalination membrane is one that has 1) the highest selectivity between water molecules and salt ions, and 2) the highest water permeability. To date, such an ideal membrane does not exist. Current water desalination membranes either have high selectivity or high water permeability but not both, which is an empirical observation commonly referred to as a performance tradeoff.[40] Over the past several decades, the search for an ideal desalination membrane has been largely empirically driven via development of new polymer selective layers with modified or entirely new chemistries. To efficiently develop an ideal membrane requires an understanding of the intimate relationships between polymer chemistry, resultant structure and membrane performance. Addressing this challenge necessitates measurements that enable the development of the structure-property relationships relevant to transport.

The state-of-the-art membrane material used in RO and NF is a polyamide (PA) thin film composite (TFC). It is a multi-component polymeric laminate consisting of three different classes of polymers: the semi-permeable layer that separates salt from water is a PA ultrathin film with a thickness ≈100 nm. It is a highly crosslinked polymer network with a mesh size <1 nm in dimensions that enables relatively higher permeation of water compared to salt ions. Directly beneath this selective layer is a porous intermediate support made of polysulfone (PSf), followed by a non-woven polyester (PET) fabric to provide mechanical support with minimal hydraulic resistance to the selective PA layer.

Desalination occurs at the dense PA selective layer according to the commonly accepted mechanism of solution-diffusion, which separates water molecules and salt ions based on permeability differences.[41] It is the product of the solubility and diffusivity that defines permeability and an intrinsic property between the particular permeating species and the membrane material. The polymer chemistry defines the membrane structure and dynamics. These two materials properties determine how permeable the selective layer is to a particular permeate, which in the case of water desalination is either water molecules or salt ions within the PA selective layer.

There are only two reported works on using reflectivity to study the swelling behavior of commercial water desalination membranes, as most water desalination membranes are not ideally suited for reflectivity measurements. High surface and interfacial roughness of the membranes will be mostly captured in the reflectivity measurements and provide little to no information pertaining to the film thickness and density of the selective PA layer.

Work by Chan and coworkers used XR to study the swelling of commercial PA selective layers.[28] In their study, the swelling behavior of an NF selective layer (Dow Filmtec NF270) was measured using XR as a function of relative humidity. To study the water absorption of the selective layer alone, the layer was separated from the PET and PSf using a delamination-dissolution procedure to adhere the PA layer onto a silicon substrate, is then measured using XR.[42]

Figure 1 summarizes the characterization of the water vapor swelling behavior of the NF270 selective layer using XR. The NF270 selective layer was mounted inside the humidity- and temperature-controlled chamber Figure 1a. Water vapor swelling measurements were performed by measuring the film thickness at different relative humidity levels ranging from 0 % RH to 95 % RH.

Figure 1b shows the XR versus scattering vector (Q) curves for the NF270 selective layer exposed to several relative humidity levels. Several key features are observed from this figure. First, the shift in the interference fringes to tighter spacing indicates that the selective layer increases in thickness with humidity. Specifically, the selective layer with an initial film thickness, h = 17.3 nm swelled to 25.8 nm at 95 % RH. Second, the critical scattering vector shifts to slightly lower Q, thus suggesting that the selective layer is absorbing water because the electron density of the selective layer is greater than that of water.

Once the swelling ratio (α) versus water activity (a_s) of the PA selective is determined, the thermodynamic parameters of the swollen polymer network can be extrapolated using the appropriate thermodynamic model. The Flory interaction parameter (χ) and the number of monomers between network junctions (N) can be extrapolated from the results shown in Figure 1d. The Flory-Rehner theory [43,44] was used to describe the swelling ratio of the polymer network with water activity. The Flory-Rehner theory describes the swelling behavior of highly swollen polymer networks with ideal network junction functionality (f=4). This model is not appropriate for networks with low swelling ratio (α<2) and non-ideal

functionality such as the PA networks of interest (f=3), which helps to explain the large N (monomers between network junctions) value obtained for the NF270 PA network. XR is limited to thin films with low roughness, which means that the measurement is best suited to desalination membranes that are relatively smooth. It is difficult to define a specific RMS roughness value below which the thin film is ideally suited for reflectivity measurements because both interfacial roughness and layer thickness affects the reflectivity data. Empirical evidence suggests that commercial NF selective layers, with RMS roughness ≈6 nm,[45] can be resolved by reflectivity whereas commercial RO selective layers, with RMS roughness ≈130 nm,[45] cannot be resolved by reflectivity due to the disappearance of the interference fringes.

To better characterize the thermodynamic parameters of these PA networks, Chan and co-workers employed a different polymer network swelling model to describe the swelling behavior of "model" PA networks synthesized via molecular layer-by-layer (mLbL) assembly.[46] The four "model" PA networks, which include poly(diethylenediamine trisamide) (P(DDTA)), poly(*m*-phenylene trisamide) (P(*m*PDTA)), poly(*o*-phenylene trisamide) (P(*o*PDTA)), and poly(*p*-phenylene trisamide) (P(*p*PDTA)), are analogs to commercial desalination membranes and consist of the same triacid chloride monomer but different diamine monomer. Thin films of the four networks were synthesized using mLbL[47,48] on Si substrates and their swelling ratios versus water vapor activity were quantified using XR in a similar procedure to their previous work.[28] (Figure 2a). The key finding is that the maximum swelling ratio, when a_s=1, is strongly dependent on the network chemistry. The maximum swelling ratio of P(DDTA) is significantly greater than P(*m*PDTA), S ≈1.50 versus S ≈1.04. This result suggests that P(DDTA) should have a higher water flux compared with P(*m*PDTA) because the water flux is a function of the water concentration within the PA membrane.[41,49] Since P(DDTA) and P(*m*PDTA) are analogs to commercial NF and RO membranes, respectively, the difference in swelling ratios is consistent with the empirical findings that show that the water flux for commercial NF membranes is significantly greater than RO membranes.[40]

Another interesting finding of this work was that the swelling behavior of these PA networks can be better described by the Painter-Shenoy theory[34] as opposed to the classic Flory-Rehner. The difference between the two models is that the Flory-Rehner model assumes a uniform water distribution throughout the film whereas the Painter-Shenoy assumes that due to non-affine swelling, there is heterogeneous water distribution throughout the film where there are water-rich regions devoid of polymer chains (Figure 2b). The researchers showed that the Painter-Shenoy model better described the swelling behavior of the PA networks as demonstrated by the more accurate values of N, which were confirmed using atomic composition analysis by X-ray photoelectron spectroscopy. This work suggests that characterizing the swelling behavior via XR is a useful approach to determine the PA network parameters. More importantly, these measurements

enable indirect characterization of the structure of these membranes, which help improve our understanding of the relationship between polymer network structure and membrane performance.

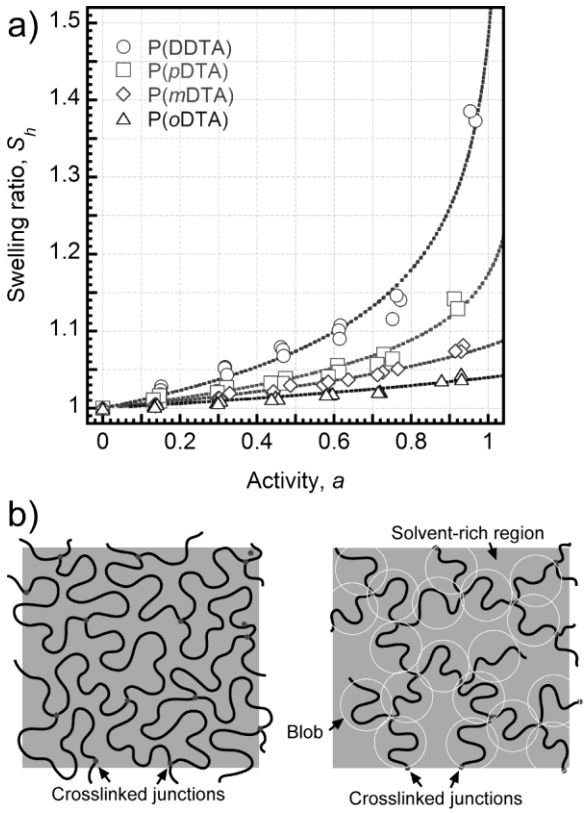

Figure 2. Studying the swelling behavior of mLbL PA desalination membrane selective layers via XR. a) Swelling ratio versus water activity for 4 mLbL PA networks. The curves are fits to the data based on Painter-Shenoy theory developed for one-dimensional swelling.[46] b) The two possible polymer network models that describe the swelling behavior of these PA networks. Reproduced with permission from reference 46. Copyright 2013 John Wiley & Sons.

Since quantifying the transport properties of a polymer film requires measurement of both the rate of swelling and absolute swelling at long times, an alternative measurement called quartz crystal microbalance with dissipation monitoring (QCM-D) can potentially provide this complete picture for ultrathin membranes. This is a gravimetric-based approach that has been used to measure

the swelling ratio of the PA selective layer as a function of water activity with high sensitivity.[50] Unlike XR, which is a slow measurement and thus cannot quantify kinetics of the swelling process, QCM-D can potentially measure the solvent uptake rate for these ultrathin films.[26,50] Commercial NF membranes were attached onto QCM-D sensors to measure the dependence of apparent diffusion coefficient and equilibrium swelling as a function of water vapor activity. The results revealed that these commercial membranes also follow the Painter-Shenoy swelling thermodynamics discussed here.[50] Due to the complexity of the commercial NF film structure, a number of mathematical approximations must be made for diffusion coefficient and solubility of the polyamide layer, as significant contributions from the hydrophilic polysulfone support layer occur, but cannot be separated from the selective PA layer in these commercial membranes.

Tailored Interfaces with High Grafting Density Polymer Brushes

Although semi-permeable membranes are currently used in numerous purification applications, they are fairly constrained in the number of tunable parameters in their design, mainly the chemistry of the membrane and the average pore size, making analyte selectivity limited to the ability to synthesize crosslinked networks with a high degree of control. On the other hand, end-grafted polymer chains, or polymer brushes, have the potential to generate tunable ultra-thin films, as chain conformation and grafting density are additional handles to control the responsiveness of the layer to small changes in the local environment, and ultimately, layer selectivity.[51–55] Polymer brushes have been previously used in synergistic combination with conventional membranes to selectively filter and separate biological species[54–56] as well as to prevent biofouling on the surface of ultrafiltration membranes without affecting desired selectivity.[56] Brushes grown inside nanopores have been demonstrated to control selectivity in gas separations.[57] A recent review article summarizes many applications of polymer brushes as membrane platforms in areas such as reverse osmosis, gas permeability, pervaporation, and protein absorption.[58] The authors hypothesize that the chemistry and morphology of polymer brushes will contribute significantly to the separation of species as these parameters will affect the selectivity of an analyte in the layer. Rigid and glassy polymers will more likely favor diffusivity of small molecules, while flexible, rubbery polymers would promote permeability of larger, more soluble species.[58] Extended chains in high grafting density brushes are predicted to enhance separation more profoundly than non-extended chains as the elongated conformation results in larger number of contacts between solvent and monomer, improving solubility.

Under limited applications, brushes have also been used to modify stationary phases and capillaries for chromatographic separations.[59–61] These studies have utilized grafted chains to modify the size and surface chemistry of stationary phase pores, changing enthalpy and entropy of small molecule interaction with the surface-bound chains.[60] Similarly to commercial RO and NF membranes, quantitative measurements of the thermodynamic parameters of polymer brush-based stationary phases is challenging on heterogeneous, rough supports, especially for systematic, *in situ* measurements of the brush response to solvent and other external stimuli.

Controlled polymer brushes grafted from a flat surface, therefore, are attractive as model materials to study solvation thermodynamics of polymer chains at a surface, with applications in developing better separation methods. High grafting density brushes can serve as model stationary phase surface with tunable interaction energy, provided that the contributions to solvation thermodynamics, such as the high local concentration of chains, limited chain entropy, grafting density, the film thickness, and the extended chain orientation can be deconvoluted. Brushes at low grafting density can also serve as proxies to individual "free" chains absorbing to a stationary phase, as has been demonstrated in the measurement and modeling of the polymer-surface interaction parameter via the swelling/collapsing of individual chains,[62] but will not be covered in this chapter.

Previous studies examining the solvation thermodynamics of polymer brushes have proved challenging as the experimentally reported polymer-solvent interaction parameter was much larger than corresponding solution values[63–65] attributed to a concentration- dependent χ parameter, where solvent quality is dependent on solvent concentration within the film.[28,66–68] Several theoretical thermodynamic models have been used to describe equilibrium swelling within polymer brushes specifically, such as scaling models[69,70], self-consistent field models[71], and mean field theory.[72–75] In each approach, the polymer-solvent interaction parameter (χ) is treated as a constant, which is measured at the maximum swollen thickness. These studies do not, however, attempt to discern whether the concentration dependence is the result of the extended chain conformation, overall film thickness, or because the polymer volume fraction for these swollen films is very high ($\phi_p > 0.5$), resulting in a highly concentrated polymer layer, where higher order interactions become significant.

In order to deconvolute the impact of chain conformation versus chain concentration on solvent quality within the films, photo cross-linked polymer thin films with known molar mass between network junctions were swollen in solvent vapor and results were compared to polymer brushes of comparable thicknesses swollen under identical conditions. The reasoning for this comparative study is threefold. First, crosslinked films are highly confined at the surface with high polymer volume fractions similar to the brushes, differing only in their lack of chain orientation. Second, thermodynamic models to determine χ for cross-linked

gels have been successfully tested by utilizing the chemical potential change within a film through vapor-phase swelling.[28,46] Finally, thermodynamics of polymer brush solvation can be probed in the vapor phase, as the scaling relationship of a swollen polymer brush ($h^* \propto N\sigma^{1/3}$, where h^* is the normalized equilibrium film thickness) derived by Alexander,[70] de Gennes,[69] and self-consistent field[71] brush models are consistent between vapor and liquid phase swelling of a polymer brush – solvent pair.[76]

XR was used to measure and compare the equilibrium swelling behavior of poly(methyl methacrylate) (PMMA) crosslinked gels and brushes in solvent vapor of increasing concentration. Two poly(methyl methacrylate) (PMMA) brushes with the same high grafting density (σ = 0.67 ± 0.02 chains/nm^2) but different dry thicknesses of (nominally) 50 nm and 100 nm were studied. These layers have brush chains with number average molar masses (M_n) of 55,000 g/mol and 105,000 g/mol, respectively (obtained by direct measurement of chains cleaved from the surface[74,77]). The PMMA brushes were synthesized using surface-initiated atom transfer radical polymerization (ATRP) similar to previous reported proceedures.[63] These brushes are in the high grafting density regime, and the normalized thickness scales with σ^n, where σ is grafting density (chains/nm^2) and n is a scaling exponent with a value greater or equal to 0.6.[78] Cross-linked thin films were synthesized with a PMMA standard (M_n = 100 kg/mol) and a photo cross-linker at comparable thicknesses to the brushes.[79] This permits measurement of the volume fraction of solvent within the films as a function of the activity and comparison of swelling between statistically cross-linked films and surface-initiated brushes with constant grafting density. The density and thickness changes of the brushes are compared to determine the dimensionality of brush swelling, and experimental data are compared to a mean-field theory to attain $\chi(\phi)$.

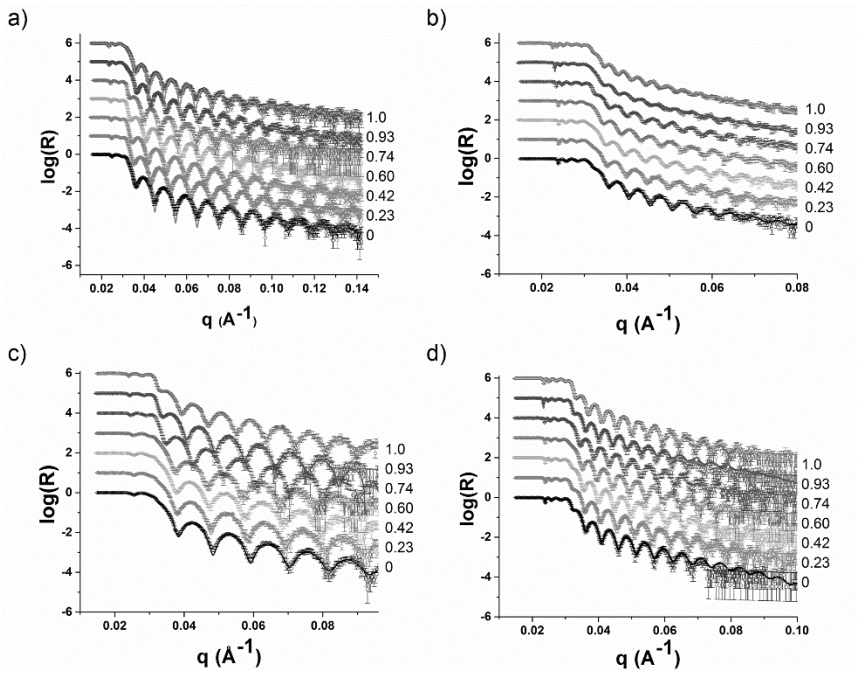

Figure 3. *Log reflectivity curves for studied PMMA films upon swelling. All plots are offset by a decade for clarity. (a) 50 nm cross-linked film (b) 100 nm cross-linked film (c) 50 nm brush film (d) 100 nm brush film. Error bars represent estimated standard deviation of the total reflectivity counts at every measured q after correcting for geometrical factors (footprint correction).*

The XR curves and curve fits for the polymer crosslinked and brush layers are shown in Figure 3. There is high reproducibility in the dry measurements, indicating that solvent was completely removed from the films during vacuum annealing before the next solvent was added and that degradation of the film was not observed.[80] All thin films were exposed to acetone vapor with $0.23 \leq a_s \leq 1$; representative X-ray reflectivity curves for (nominally) 50 nm and 100 nm thick dry layer for cross-linked and brush films in the dry and swollen states are shown in Figure 3. In all samples, a decrease in the critical angle was observed with increasing solvent activity and thickness increased, as evidenced by the shift in fringes to lower scattering vector values. All data was fit to a single layer model shown as the solid line over the scattering data (open symbols).

Thickness and volumetric swelling ratios were determined from h and Q_c^2 values based on equations 2-4. The initial solvent volume fraction (ϕ_s) calculated

for all measured films for activites between 0.23 and 0.60 were less than zero (data not shown). Initial evaluation of ϕ_s may appear as if the film is contracting, as contracting films can have an apparent 'negative' solvent fraction at low activities, as has been observed[81] and simulated[82] in swelling of grafted DNA chains in a low humidity environment. However, the film thicknesses (h) measured here always increase relative to the dry state with increasing solvent activity, which indicate that the brushes and cross-linked networks do not contract. These 'contradictory' observations, where film thicknesses increases, but the electron density of the film also increases (resulting in negative ϕ_s) can be attributed to how polymer volume fraction is defined in equation 3 relative to the electron density of the dry polymer ($Q_c^2{}_{dry}$). Initial polymer volume fraction, in the dry state, is defined as unity in equation 3, and cannot account for pores or small, localized heterogeneities in the film which interact with solvent non-ideally until they dissipate as the film begins to swell. The heterogeneities are likely due to either non-initiated sites (and resulting polymeriztion defects), or localized chain plasticization, that may allow trace amounts of solvent to penetrate the film, but do not substanially affect the film thickness overall. Defects in polymer brushes have been previously observed in surface-initiated brushes resulting in voids or nanoinclusions within the dry layer.[83–85] While these observations have only a small effect on determining the initial electron density in the films, accurate quantification is critical to determine the actual solvent content within the film and measure the thermodynamic changes within the layer.

X-ray porosimetry measurements have been previously used to quantify porosity in organic thin films as they swell.[74,86] Determination of the volume fraction of defects in the film, or film porosity (*P*) based on reflectivity measurements in the dry and fully swollen state (denoted by the subscript *sat*, for saturated), are shown in equations 12 and 13, repectively. Equations 12 and 13 are solved simultaneously by the rule of mixtures for two unknowns, *P* and $Q_c^2{}_{poly}$. $Q_c^2{}_{N2}$ is the scattering length density of nitrogen atmosphere, which should occupy any pores in the initial (dry) state.

$$Q_{c\,dry}^2 = (1-P)Q_{c\,poly}^2 + PQ_{c\,N2}^2 \tag{12}$$

$$P = \frac{Q_{c\,sat}^2 h_{sat} - Q_{c\,dry}^2 h_{dry}}{Q_{c\,solvent}^2 h_{dry}} - \frac{h_{sat} - h_{dry}}{h_{dry}} \tag{13}$$

Once *P* and $Q_c^2{}_{poly}$, were determined, the corrected value of $Q_c^2{}_{poly}$ replaces $Q_c^2{}_{dry}$ in equation 3 to determine the actual values of ϕ_p, and as a result, ϕ_s. A summary of the resulting SLD, mass density, and *P* values for each film are shown in Table 1 and the plots of corrected ϕ_s and α as a function of activity (a_s), as are shown in Figure 4.

Table 1. Summary of Porosity within PMMA Thin Films*

Sample	$Q^2_{c\,dry}$ *(x 10 ^{5} Å^{-2})*	*Dry Thickness, h_0 (nm)*	$Q^2_{c\,poly}$ *(x 10 ^{5} Å^{-2})*	$\rho_{m_{poly}}$ *(g/cm^3)*	*P*
50 nm cross-linked	1.06 ± 5.6 x 10^{-3}	57.3 ± 0.5	1.095 ± 0.1	1.20	0.029
100 nm cross-linked	1.07 ± 3.8 x 10^{-3}	106.3 ± 2.1	1.138 ± 0.02	1.24	0.057
50 nm brush	1.10 ± 1.2 x 10^{-2}	49.5 ± 2.6	1.156 x ± 0.02	1.26	0.051
100 nm brush	1.08 ± 4.9 x 10^{-3}	100.9 ± 3.8	1.150 ± 0.002	1.26	0.064
Theoretical (bulk)			1.08	1.18	0

* ± value represents one standard deviation of the data among all trials

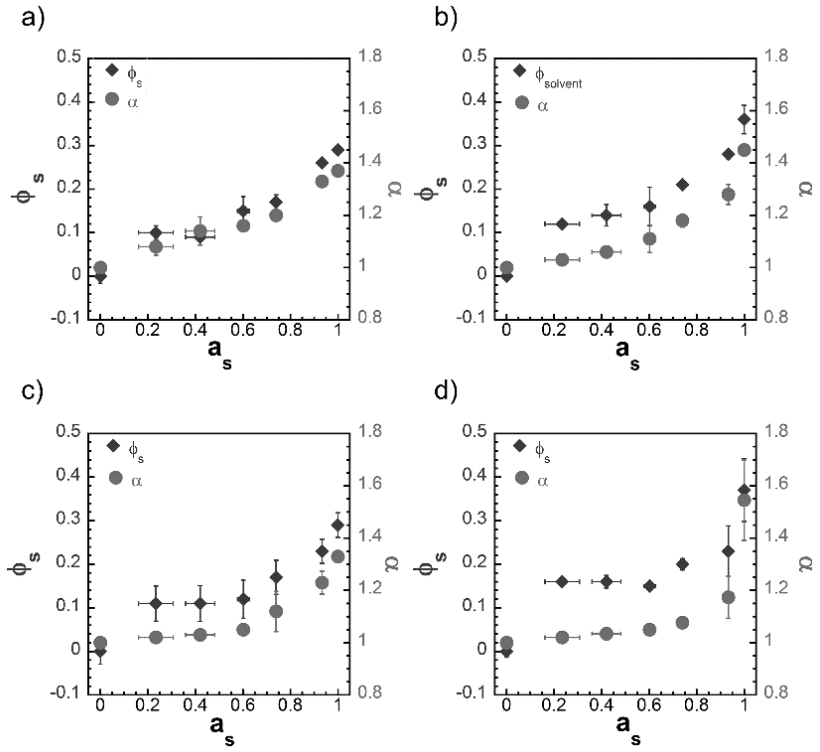

Figure 4. *Solvent uptake in thin films as a function of activity: corrected volume fraction of acetone (ϕ_s) & thickness swelling ratio (α) for 50 nm cross-linked films (a) 100 nm cross-linked films (b) 50 nm brush films (c), and 100 nm brush films (d). The error bars represent one standard deviation among all trials.*

The resulting mass density, calculated from Q_c^2, of all cross-linked and brush films are significantly greater than expected theoretical values for PMMA, with the greatest increase in material density for the polymer brushes. While the 50 nm cross-linked films have a slightly smaller volume fraction due to pores in the dry state, the remaining films have pores that comprise approximately 5-6% of the total film volume.

Swelling results were first fit to the Flory-Huggins model to determine if $\chi(\phi_p)$ can be adequately fit without inclusion of an elastic correction and as a baseline of comparison to the values when elastic corrections are applied. To determine $\chi(\phi_p)$ for the 50 nm and 100 nm crosslinked films and brushes a_s versus ϕ_p was plotted to determine the terms for χ_0, χ_1, and χ_2 (Figure 5). Prior work on characterizing the χ of linear PMMA at high polymer content ($0.72 \leq \phi_p \leq 0.95$) demonstrated a linear concentration dependent term in $\chi(\phi_p)$ for PMMA.[87] Previous studies have indicated that within highly concentrated thin films, there may be a concentration dependence to χ,[67] which may be represented by a polynomial function.[28,88] Using only two terms to fit $\chi(\phi_p)$ did not result in in a good fit of the experimental data, so an additional term, χ_2, was added to the fit parameters.

$$\chi(\phi_p) = \chi_0 + \chi_1\phi_p + \chi_2(\phi_p)^2 \tag{14}$$

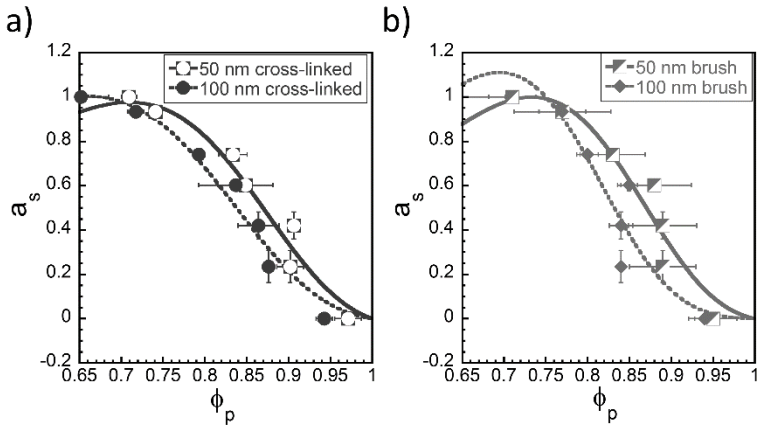

Figure 5. *Polymer volume fraction versus activity plots comparing crosslinked films (a) to polymer brushes (b). The equations on the graph represent the fit of the concentration-dependent χ parameter for each 50 nm and 100 nm film. The error bars represent one standard deviation among all trials.*

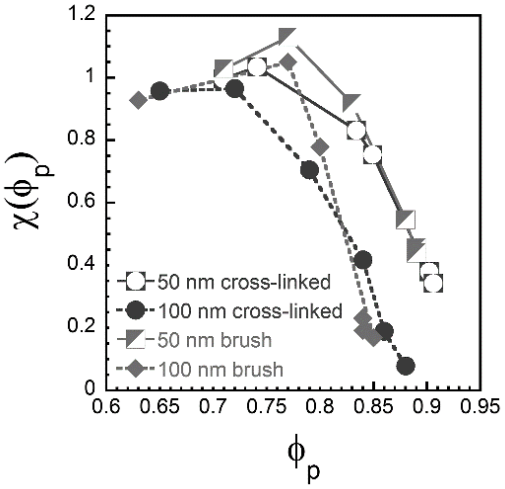

Figure 6. *Concentration-dependent Flory-Huggins interaction parameter as a function of polymer volume fraction for cross-linked and brush films.*

The resulting fits of the Flory-Huggins equation (equations 6 and 7) with concentration dependent swelling (equation 14) are shown as the solid and dashed lines in Figure 5a and 5b. The resulting $\chi(\phi_p)$ values from the fits are shown in Figure 6. As the PMMA films swell and ϕ_p decreases, $\chi(\phi_p)$ increases and plateaus at a value of approximately 1, which is greater than the literature value for PMMA in acetone of 0.46.[89] There is not a significant difference between $\chi(\phi_p)$ for the brushes and cross-linked films of comparable thicknesses. Comparison of the 50 nm and 100 nm films, however, indicates that the 50 nm films have larger initial $\chi(\phi_p)$ relative to the comparative 100 nm films, where the $\chi(\phi_p)$ converge at maximum film swelling (a_s =1). The trend in $\chi(\phi_p)$ for both cross-linked and brush films does not follow what is observed in unattached PMMA at high polymer concentrations,[87] where $\chi(\phi_p)$ decreases with decreasing ϕ_p. The films in this study resist the addition of more solvent the more they swell. This indicates that there is likely an elastic contribution to the chemical potential change that resists swelling, suggesting that a thermodynamic model such as Flory Rehner or Painter Shenoy may be appropriate to describe brush swelling and compare to thin film gels arising from the similarities these two systems share. Both crosslinked and brush films are highly confined and contain high polymer concentrations. Additional solvent in the brushes relative to the cross-linked films of comparable

thickness was not observed as was predicted. Therefore, a comparative study between the two was intended to elucidate any effects of the conformation of chains on solvent quality in these systems;[58] random orientation and crosslinks for the network and elongating chains for the brush that are extended away from the substrate surface. In essence, we are treating the polymer brush as a gel, with crosslinks at the surface boundary, and the untethered chain ends as 'dangling ends,' free to swell, encumbered by only excluded volume restrictions to chain extensions and any chain entanglements present in the brush.

To determine $\chi(\phi_p)$ for the 50 nm and 100 nm crosslinked films and brushes using the Flory Rehner model, $\ln(a_s)$ vs ϕ_p was fit to the Flory-Rehner equation (equation 9). The molar mass between crosslinks, N, used in the Flory-Rehner equation, was determined from known crosslinking density in the networks and the degree of polymerization of the brushes, which was measured by gel permeation chromatography of the recovered chains cleaved from the surface and calibrated against narrow dispersity PMMA molar mass standards. $\chi(\phi_p)$ values obtained from Flory-Rehner modeling were statistically insignificant to those obtained from Flory-Huggins theory, as the results only differ by less than 2% for all measured swelling.

The initial presence of pores in the film can potentially result in solvent-rich regions in the networks and brushes, so the Painter-Shenoy model (equations 10 and 11) was fit to the data to determine if the elastic contribution to swelling is not affine and the resultant impact on the χ parameter. Network functionality was trifunctional for the benzophenone-based crosslinks in the gel (f=3) and difunctional for the polymer brushes (f=2). $\chi(\phi_p)$ determined based on the Painter-Shenoy thermodynamic model did not yield a statistically significant different value than that from conventional Flory-Huggins, with all $\chi(\phi_p)$ values agreeing within 3%.

Comparison of crosslinked and brush film swelling shows a larger dependence on thickness than on chain orientation (random crosslinks or brush), indicating solvation is not significantly affected by how the chains in these systems are immobilized. The Painter Shenoy and Flory-Rehner mean field models for the elastic contribution to the chemical potential change do not demonstrate a significant difference from conventional Flory-Huggins theory. This result is unexpected, as the films only swell to approximately 1.5 times their dry thickness, and the swelling films resist the addition of more solvent, as observed by the plateau of $\chi(\phi_p)$ at approximately a value of 1. Attempts to fit experimental data to a Gaussian chain extension model[73] for end-grafted brushes yielded similar $\chi(\phi_p)$ results as well.

A potential explanation of these observations could be due to different glassy dynamics of these ultra-thin ($\leq$ 100 nm) PMMA films. Glass transition temperatures for PMMA have been previously demonstrated to increase with decreasing film thickness.[90] Solvent-induced glass transitions have been previously reported in grafted polymer thin films[91,92] and has been previously

observed with vapor sorption in cross-linked rubbery films[88] and polymer films below their glass transition temperature,[38] where films display a dual-mode type absorption near the glass transition. Below the glass transition, the films display a Langmuir-type adsorption and after enough solvent in the film induces the swelling to follow conventional Flory-Huggins mixing.[93] A recent study of polystyrene brushes mapped across grafting density and degree of polymerization regimes demonstrate a substantial increase in T_g at ultra-high grafting densities and low degrees of polymerization.[94] The breadth of these previous studies highlight the need to evalute dynamics of dry and solvated thin films going forward, focusing on smaller, incremental chemical potential changes and using complementary reflectivity techniques such as XR and NR to provide improved contrast.

Conclusions and Outlook

Gaining a comprehensive understanding of the structure-property-performance relationships of advanced polymer thin film networks and brushes requires application of multiple measurement methods to determine how the chemistry and molecular architecture of these materials influence the solvent interaction, selectivity, and diffusivity. In this chapter, X-ray reflectivity measurements of thin films are applied to studying the structure and dynamics of dense and ultrathin polymer layers used as model materials for water desalination and advanced chromatography applications. XR provides clear, reproducible measurements of solvent uptake in these films as a function of activity, allowing swelling experiments to be compared to established mean-field thermodynamic models.

Other scattering methods such as small-angle neutron scattering (SANS) and x-ray scattering (SAXS), ultra-high resolution SANS (USANS), or phase analysis light scattering (PALS) can be used to study longer size scale interactions in polymer thin films, although currently these have been employed on a limited basis. These techniques are not limited to the low angles of X-ray and neutron reflectivity (NR). However, the main limitation for these types of measurements is that a larger thickness of sample is usually required to obtain good scattering statistics. We have discussed the application of XR for measuring the swelling behavior of thin film polymer networks and brushes. XR and NR are great techniques for thin films but they infer the polymer network structure based on the extrapolated thermodynamic parameters, and do not directly measure any specific polymer length-scales such as the polymer mesh size. This limitation emphasizes the need to select appropriate models to interpret measurements, based on known chemistry and architecture of the films, previous experiments, and theoretical simulations.

The design and use of tunable, controlled, well-defined experimental model systems can be a useful bridge when trying to deconvolute multiple contributions to thin film thermodynamics, especially when commercial systems are 1) unavailable or 2) highly variable between samples. However, advancing thin film measurements from a fundamental research laboratory to a useful tool for designing better commercial materials requires measurements that are able to measure industrial prototypes and perform routine test measurements as well. Experimental model systems can help develop and evaluate new measurements and theoretical models, but ultimately, enhanced detection limits as well as new, high-throughput measurements for ultra-thin polymer films will be the key to making tunable coatings commercially viable in the future.

AUTHOR INFORMATION

Corresponding Authors

*Kathryn L Beers. kathryn.beers@nist.gov and Edwin P. Chan. edwin.chan@nist.gov.

Disclaimer

Certain commercial equipment, instruments, or materials are identified in this paper to specify adequately the experimental procedure. Such identification does not imply recommendation or endorsement by the National Institute of Standards and Technology, nor does it imply that the materials or equipment identified are necessarily the best available for the purpose.

References

(1) Werber, J. R.; Osuji, C. O.; Elimelech, M. Materials for next-Generation Desalination and Water Purification Membranes. *Nat. Rev. Mater.* **2016**, *1* (5), 16018.

(2) Ong, C. S.; Goh, P. S.; Lau, W. J.; Misdan, N.; Ismail, A. F. Nanomaterials for Biofouling and Scaling Mitigation of Thin Film

Composite Membrane: A Review. *Desalination* **2016**, *393*, 2–15.
(3) Lau, W. J.; Gray, S.; Matsuura, T.; Emadzadeh, D.; Paul Chen, J.; Ismail, A. F. A Review on Polyamide Thin Film Nanocomposite (TFN) Membranes: History, Applications, Challenges and Approaches. *Water Res.* **2015**, *80*, 306–324.
(4) Wang, L.; Boutilier, M. S. H.; Kidambi, P. R.; Jang, D.; Hadjiconstantinou, N. G.; Karnik, R. Fundamental Transport Mechanisms, Fabrication and Potential Applications of Nanoporous Atomically Thin Membranes. *Nat. Nanotechnol.* **2017**, *12* (6), 509–522.
(5) Stamatialis, D. F.; Papenburg, B. J.; Gironés, M.; Saiful, S.; Bettahalli, S. N. M.; Schmitmeier, S.; Wessling, M. Medical Applications of Membranes: Drug Delivery, Artificial Organs and Tissue Engineering. *J. Memb. Sci.* **2008**, *308* (1–2), 1–34.
(6) Lenhart, J. L.; Wu, W. Deviations in the Thermal Properties of Ultrathin Polymer Network Films. *Macromolecules* **2002**, *35* (13), 5145–5152.
(7) Lan, T.; Torkelson, J. M. Fragility-Confinement Effects: Apparent Universality as a Function of Scaled Thickness in Films of Freely Deposited, Linear Polymer and Its Absence in Densely Grafted Brushes. *Macromolecules* **2016**, *49* (4), 1331–1343.
(8) Lenhart, J. L.; Wu, W. Influence of Cross-Link Density on the Thermal Properties of Thin Polymer Network Films. *Langmuir* **2003**, *19*, 4863–4865.
(9) Vogt, B. D.; Prabhu, V. M.; Soles, C. L.; Satija, S. K.; Lin, E. K.; Wu, W. L. Control of Moisture at Buried Polymer/alumina Interfaces through Substrate Surface Modification. *Langmuir* **2005**, *21* (6), 2460–2464.
(10) Nguyen, H. K.; Labardi, M.; Lucchesi, M.; Rolla, P.; Prevosto, D. Plasticization in Ultrathin Polymer Films: The Role of Supporting Substrate and Annealing. *Macromolecules* **2013**, *46* (2), 555–561.
(11) Vogt, B. D.; Soles, C. L.; Lee, H.-J.; Lin, E. K.; Wu, W. Moisture Absorption into Ultrathin Hydrophilic Polymer Films on Different Substrate Surfaces. *Polymer (Guildf).* **2005**, *46* (5), 1635–1642.
(12) Gibaud, A.; Vignaud, G. Specular Reflectivity from Smooth and Rough Surfaces. In *X-ray and Neutron Reflectivity*; Springer Berlin Heidelberg: Berlin, Heidelberg; pp 85–131.
(13) Russell, T. P. X-Ray and Neutron Reflectivity for the Investigation of Polymers. *Mater. Sci. Reports* **1990**, *5* (4), 171–271.
(14) Lin, E. K.; Soles, C. L.; Goldfarb, D. L.; Trinque, B. C.; Burns, S. D.; Jones, R. L.; Lenhart, J. L.; Angelopoulos, M.; Willson, C. G.; Satija, S. K.; et al. Direct Measurement of the Reaction Front in Chemically Amplified Photoresists. *Science (80-.).* **2002**, *297* (5580), 372–375.
(15) Orts, W. J.; van Zanten, J. H.; Wu, W.; Satija, S. K. Observation of Temperature Dependent Thicknesses in Ultrathin Polystyrene Films on Silicon. *Phys. Rev. Lett.* **1993**, *71* (6), 867–870.

(16) Wu, W.; Wallace, W. E.; van Zanten, J. H.; Bauer, B. J.; Liu, D.; Wong, A. Diffusion of Linear Polystyrene into Crosslinked Polystyrene. *Polymer (Guildf).* **1997**, *38* (11), 2583–2594.
(17) Wang, J.; Tolan, M.; Seeck, O. H.; Sinha, S. K.; Bahr, O.; Rafailovich, M. H.; Sokolov, J. Surfaces of Strongly Confined Polymer Thin Films Studied by X-Ray Scattering. *Phys. Rev. Lett.* **1999**, *83* (3), 564–567.
(18) Lee, H.-J.; Soles, C. L.; Ro, H. W.; Hines, D. R.; Jones, R. L.; Lin, E. K.; Karim, A.; Wu, W. Characterizing Nanoimprint Pattern Cross-Section and Fidelity from X-Ray Reflectivity. In *Proceedings of the SPIE*; 2006; Vol. 6151, pp 183–189.
(19) Lee, H.-J.; Soles, C. L.; Ro, H. W.; Jones, R. L.; Lin, E. K.; Wu, W.; Hines, D. R. Nanoimprint Pattern Transfer Quality from Specular X-Ray Reflectivity. *Appl. Phys. Lett.* **2005**, *87* (26), 263111.
(20) Foster, M.; Stamm, M.; Reiter, G. X-Ray Reflectometer for Study of Polymer Thin Films and Interfaces. *Vacuum* **1990**, *41* (4–6), 1441–1444.
(21) Papra, A.; Gadegaard, N.; Larsen, N. B. Characterization of Ultrathin Poly(ethylene Glycol) Monolayers on Silicon Substrates. *Langmuir* **2001**, *17* (5), 1457–1460.
(22) Singh, A.; Mukherjee, M. Swelling Dynamics of Ultrathin Polymer Films. *Macromolecules* **2003**, *36* (23), 8728–8731.
(23) Mukherjee, M.; Singh, A.; Daillant, J.; Menelle, A.; Cousin, F. Effect of Solvent−Polymer Interaction in Swelling Dynamics of Ultrathin Polyacrylamide Films: A Neutron and X-Ray Reflectivity Study. *Macromolecules* **2007**, *40* (4), 1073–1080.
(24) Schmitt, J.; Gruenewald, T.; Decher, G.; Pershan, P. S.; Kjaer, K.; Loesche, M. Internal Structure of Layer-by-Layer Adsorbed Polyelectrolyte Films: A Neutron and X-Ray Reflectivity Study. *Macromolecules* **1993**, *26* (25), 7058–7063.
(25) Decher, G. Fuzzy Nanoassemblies: Toward Layered Polymeric Multicomposites. *Science (80-.).* **1997**, *277* (5330), 1232–1237.
(26) Eastman, S. A.; Kim, S.; Page, K. A.; Rowe, B. W.; Kang, S.; Soles, C. L.; Yager, K. G. Effect of Confinement on Structure, Water Solubility, and Water Transport in Nafion Thin Films. *Macromolecules* **2012**, *45* (19), 7920–7930.
(27) Pedersen, J. S.; Hamley, I. W. Analysis of Neutron and X-Ray Reflectivity Data. II. Constrained Least-Squares Methods. *J. Appl. Crystallogr.* **1994**, *27* (1), 36–49.
(28) Chan, E. P.; Young, A. P.; Lee, J.-H.; Chung, J. Y.; Stafford, C. M. Swelling of Ultrathin Crosslinked Polyamide Water Desalination Membranes. *J. Polym. Sci. Part B Polym. Phys.* **2013**, *51* (6), 385–391.
(29) Soles, Christopher L. ; Lin, Eric K.; Lee, H.-J. ; W.; U, W. NIST Manuscript Publication Search. *Pore Charact. Low-k Dielectr. Film. Using X-ray Reflectivity X-ray Porosim. (SP 960-13)* **2004**, *33(1)*.

(30) Kienzle, P. A.; O'Donovan, K. V.; Ankner, J. F.; Berk, N. F.; Majkrzak, C. F. Reflpak http://www.ncnr.nist.gov/reflpak. (accessed Feb 2, 2018).
(31) Kienzle, P. A. Neutron Activation Calculator http://www.ncnr.nist.gov/resources/activation/ (accessed Feb 2, 2018).
(32) Kennedy, J. W. Principles of Polymer Chemistry. *J. Am. Chem. Soc.* **1954**, *76* (10), 2854.
(33) Flory, P. J.; Rehner, J. Statistical Mechanics of Cross-Linked Polymer Networks II. Swelling. *J. Chem. Phys.* **1943**, *11* (11), 521.
(34) Painter, P. C.; Shenoy, S. L. A Simple Model for the Swelling of Polymer Networks. *J. Chem. Phys.* **1993**, *99* (2), 1409–1418.
(35) Toomey, R.; Freidank, D.; Rühe, J. Swelling Behavior of Thin, Surface-Attached Polymer Networks. *Macromolecules* **2004**, *37* (3), 882–887.
(36) Manoli, K.; Goustouridis, D.; Chatzandroulis, S.; Raptis, I.; Valamontes, E. S.; Sanopoulou, M. Vapor Sorption in Thin Supported Polymer Films Studied by White Light Interferometry. *Polymer (Guildf).* **2006**, *47* (17), 6117–6122.
(37) McKenna, G. B.; Flynn, K. M.; Chen, Y. Swelling in Crosslinked Natural Rubber: Experimental Evidence of the Crosslink Density Dependence of χ. *Polymer (Guildf).* **1990**, *31* (10), 1937–1945.
(38) Russell, S. .; Weinkauf, D. . Vapor Sorption in Plasma Polymerized Vinyl Acetate and Methyl Methacrylate Thin Films. *Polymer (Guildf).* **2001**, *42* (7), 2827–2836.
(39) Shannon, M. A.; Bohn, P. W.; Elimelech, M.; Georgiadis, J. G.; Marinas, B. J.; Mayes, A. M. Science and Technology for Water Purification in the Coming Decades. *Nature* **2008**, *452* (7185), 301–310.
(40) Geise, G. M.; Park, H. B.; Sagle, A. C.; Freeman, B. D.; McGrath, J. E. Water Permeability and Water/salt Selectivity Tradeoff in Polymers for Desalination. *J. Memb. Sci.* **2011**, *369* (1–2), 130–138.
(41) Paul, D. R. Reformulation of the Solution-Diffusion Theory of Reverse Osmosis. *J. Memb. Sci.* **2004**, *241* (2), 371–386.
(42) Chung, J. Y.; Lee, J.-H.; Beers, K. L.; Stafford, C. M. Stiffness, Strength, and Ductility of Nanoscale Thin Films and Membranes: A Combined Wrinkling–Cracking Methodology. *Nano Lett.* **2011**, *11* (8), 3361–3365.
(43) Flory, P. J.; Rehner, J. Statistical Mechanics of Cross-Linked Polymer Networks I. Rubberlike Elasticity. *J. Chem. Phys.* **1943**, *11* (11), 512–520.
(44) Flory, P. J.; Rehner, J. Statistical Mechanics of Cross-Linked Polymer Networks II. Swelling. *J. Chem. Phys.* **1943**, *11* (11), 521–526.
(45) Lee, J.-H.; Chung, J. Y.; Chan, E. P.; Stafford, C. M. Correlating Chlorine-Induced Changes in Mechanical Properties to Performance in Polyamide-Based Thin Film Composite Membranes. *J. Memb. Sci.* **2013**, *433*, 72–79.

(46) Chan, E. P.; Young, A. P.; Lee, J.-H.; Stafford, C. M. Swelling of Ultrathin Molecular Layer-by-Layer Polyamide Water Desalination Membranes. *J. Polym. Sci. Part B Polym. Phys.* **2013**, *51* (22), 1647–1655.
(47) Johnson, P. M.; Yoon, J.; Kelly, J. Y.; Howarter, J. A.; Stafford, C. M. Molecular Layer-by-layer Deposition of Highly Crosslinked Polyamide Films. *J. Polym. Sci. Part B Polym. Phys.* **2012**, *50* (3), 168–173.
(48) Chan, E. P.; Lee, J.-H.; Chung, J. Y.; Stafford, C. M. An Automated Spin-Assisted Approach for Molecular Layer-by-Layer Assembly of Crosslinked Polymer Thin Films. *Rev. Sci. Instrum.* **2012**, *83* (11), 114102-114102–114106.
(49) Paul, D. R.; Ebra-Lima, O. M. Pressure-Induced Diffusion of Organic Liquids through Highly Swollen Polymer Membranes. *J. Appl. Polym. Sci.* **1970**, *14* (9), 2201–2224.
(50) Nadermann, N. K.; Chan, E. P.; Stafford, C. M. Bilayer Mass Transport Model for Determining Swelling and Diffusion in Coated, Ultrathin Membranes. *ACS Appl. Mater. Interfaces* **2015**, *7* (6), 3492–3502.
(51) Brittain, W. J.; Minko, S. A Structural Definition of Polymer Brushes. *J. Polym. Sci. Part A Polym. Chem.* **2007**, *45* (16), 3505–3512.
(52) Azzaroni, O. Polymer Brushes Here, There, and Everywhere: Recent Advances in Their Practical Applications and Emerging Opportunities in Multiple Research Fields. *J. Polym. Sci. Part A Polym. Chem.* **2012**, *50* (16), 3225–3258.
(53) Chen, T.; Ferris, R.; Zhang, J.; Ducker, R.; Zauscher, S. Stimulus-Responsive Polymer Brushes on Surfaces: Transduction Mechanisms and Applications. *Prog. Polym. Sci.* **2010**, *35* (1–2), 94–112.
(54) Ayres, N. Polymer Brushes: Applications in Biomaterials and Nanotechnology. *Polym. Chem.* **2010**, *1* (6), 769.
(55) Jain, P.; Baker, G. L.; Bruening, M. L. Applications of Polymer Brushes in Protein Analysis and Purification. *Annu. Rev. Anal. Chem. (Palo Alto. Calif).* **2009**, *2*, 387–408.
(56) Bernstein, R.; Singer, C. E.; Singh, S. P.; Mao, C.; Arnusch, C. J. UV Initiated Surface Grafting on Polyethersulfone Ultrafiltration Membranes via Ink-Jet Printing-Assisted Modification. *J. Memb. Sci.* **2018**, *548*, 73–80.
(57) Bruening, M. L.; Dotzauer, D. M.; Jain, P.; Ouyang, L.; Baker, G. L. Creation of Functional Membranes Using Polyelectrolyte Multilayers and Polymer Brushes. *Langmuir* **2008**, *24* (15), 7663–7673.
(58) Keating, J. J.; Imbrogno, J.; Belfort, G. Polymer Brushes for Membrane Separations: A Review. *ACS Appl. Mater. Interfaces* **2016**, *8* (42), 28383–28399.
(59) Miller, M. D.; Baker, G. L.; Bruening, M. L. Polymer-Brush Stationary Phases for Open-Tubular Capillary Electrochromatography. *J.*

Chromatogr. A **2004**, *1044* (1–2), 323–330.
(60) Mizutani, A.; Nagase, K.; Kikuchi, A.; Kanazawa, H.; Akiyama, Y.; Kobayashi, J.; Annaka, M.; Okano, T. Thermo-Responsive Polymer Brush-Grafted Porous Polystyrene Beads for All-Aqueous Chromatography. *J. Chromatogr. A* **2010**, *1217* (4), 522–529.
(61) Slater, M.; Snauko, M.; Svec, F.; Fréchet, J. M. J. "Click Chemistry" in the Preparation of Porous Polymer-Based Particulate Stationary Phases for Mu-HPLC Separation of Peptides and Proteins. *Anal. Chem.* **2006**, *78* (14), 4969–4975.
(62) Sheridan, R. J.; Orski, S. V.; Jones, R. L.; Satija, S. K.; Beers, K. L. Surface Interaction Parameter Measurement of Solvated Polymers via Model End-Tethered Chains. *Macromolecules* **2017**, *50* (17), 6668–6678.
(63) Orski, S. V.; Sheridan, R. J.; Chan, E. P.; Beers, K. L. Utilizing Vapor Swelling of Surface-Initiated Polymer Brushes to Develop Quantitative Measurements of Brush Thermodynamics and Grafting Density. *Polymer (Guildf).* **2015**, *72*, 471–478.
(64) Biesalski, M.; Rühe, J. Swelling of a Polyelectrolyte Brush in Humid Air. *Langmuir* **2000**, *16* (4), 1943–1950.
(65) Galvin, C. J.; Dimitriou, M. D.; Satija, S. K.; Genzer, J. Swelling of Polyelectrolyte and Polyzwitterion Brushes by Humid Vapors. *J. Am. Chem. Soc.* **2014**, *136* (36), 12737–12745.
(66) Evans, R.; Napper, D. H. Perturbation Method for Incorporating the Concentration Dependence of the Flory–Huggins Parameter into the Theory of Steric Stabilization. *J. Chem. Soc. Faraday Trans. 1 Phys. Chem. Condens. Phases* **1977**, *73*, 1377.
(67) Baulin, V. A.; Halperin, A. Signatures of a Concentration-Dependent Floryχ Parameter: Swelling and Collapse of Coils and Brushes. *Macromol. Theory Simulations* **2003**, *12* (8), 549–559.
(68) Baulin, V. A.; Halperin, A. Concentration Dependence of the Flory χ Parameter within Two-State Models. *Macromolecules* **2002**, *35* (16), 6432–6438.
(69) de Gennes, P. G. Conformations of Polymers Attached to an Interface. *Macromolecules* **1980**, *13* (5), 1069–1075.
(70) Alexander, S. Adsorption of Chain Molecules with a Polar Head a Scaling Description. *J. Phys.* **1977**, *38* (8), 983–987.
(71) Milner, S. T.; Witten, T. A.; Cates, M. E. Theory of the Grafted Polymer Brush. *Macromolecules* **1988**, *21* (8), 2610–2619.
(72) Zhulina, E. B.; Borisov, O. V.; Pryamitsyn, V. A.; Birshtein, T. M. Coil-Globule Type Transitions in Polymers. 1. Collapse of Layers of Grafted Polymer Chains. *Macromolecules* **1991**, *24* (1), 140–149.
(73) Birshtein, T. M.; Lyatskaya, Y. V. Theory of the Collapse-Stretching Transition of a Polymer Brush in a Mixed Solvent. *Macromolecules*

1994, *27* (5), 1256–1266.
(74) Kang, C.; Crockett, R. M.; Spencer, N. D. Molecular-Weight Determination of Polymer Brushes Generated by SI-ATRP on Flat Surfaces. *Macromolecules* **2014**, *47* (1), 269–275.
(75) Espinosa-Marzal, R. M.; Nalam, P. C.; Bolisetty, S.; Spencer, N. D. Impact of Solvation on Equilibrium Conformation of Polymer Brushes in Solvent Mixtures. *Soft Matter* **2013**, *9* (15), 4045.
(76) Sun, L.; Akgun, B.; Hu, R.; Browning, J. F.; Wu, D. T.; Foster, M. D. Scaling Behavior and Segment Concentration Profile of Densely Grafted Polymer Brushes Swollen in Vapor. *Langmuir* **2016**, *32* (22), 5623.
(77) Patil, R. R.; Turgman-Cohen, S.; Šrogl, J.; Kiserow, D.; Genzer, J. Direct Measurement of Molecular Weight and Grafting Density by Controlled and Quantitative Degrafting of Surface-Anchored Poly(methyl Methacrylate). *ACS Macro Lett.* **2015**, *4* (2), 251–254.
(78) Moh, L. C. H.; Losego, M. D.; Braun, P. V. Solvent Quality Effects on Scaling Behavior of Poly(methyl Methacrylate) Brushes in the Moderate- and High-Density Regimes. *Langmuir* **2011**, *27* (7), 3698–3702.
(79) Orski, S. V.; Kundu, S.; Gross, R.; Beers, K. L. Design and Implementation of Two-Dimensional Polymer Adsorption Models: Evaluating the Stability of Candida Antarctica Lipase B/solid-Support Interfaces by Qcm-D. *Biomacromolecules* **2013**, *14* (2), 377–386.
(80) Brown, H. R.; Char, K.; Deline, V. R. Enthalpy-Driven Swelling of a Polymer Brush. *Macromolecules* **1990**, *23* (13), 3383–3385.
(81) Mertens, J.; Rogero, C.; Calleja, M.; Ramos, D.; Martín-Gago, J. A.; Briones, C.; Tamayo, J. Label-Free Detection of DNA Hybridization Based on Hydration-Induced Tension in Nucleic Acid Films. *Nat. Nanotechnol.* **2008**, *3* (5), 301–307.
(82) Wagman, M.; Medalion, S.; Rabin, Y. Anomalous Swelling of Polymer Monolayers by Water Vapor. *Macromolecules* **2012**, *45* (23), 9517–9521.
(83) Kim, J. U.; O'Shaughnessy, B. Nanoinclusions in Dry Polymer Brushes. *Macromolecules* **2006**, *39* (1), 413–425.
(84) Lu, X.; Yan, Q.; Ma, Y.; Guo, X.; Xiao, S.-J. Growing Embossed Nanostructures of Polymer Brushes on Wet-Etched Silicon Templated via Block Copolymers. *Sci. Rep.* **2016**, *6* (1), 20291.
(85) Santer, S.; Rühe, J. Motion of Nano-Objects on Polymer Brushes. *Polymer (Guildf).* **2004**, *45* (25), 8279–8297.
(86) Lee, H.-J.; Soles, C. L.; Liu, D.-W.; Bauer, B. J.; Lin, E. K.; Wu, W.; Grill, A. Structural Characterization of Porous Low- *K* Thin Films Prepared by Different Techniques Using X-Ray Porosimetry. *J. Appl. Phys.* **2004**, *95* (5), 2355–2359.
(87) Lai, J.-Y.; Lin, S.-F.; Lin, F.-C.; Wang, D.-M. Construction of Ternary

Phase Diagrams in nonsolvent/solvent/PMMA Systems. *J. Polym. Sci. Part B Polym. Phys.* **1998**, *36* (4), 607–615.
(88) Singh, A.; Freeman, B. D.; Pinnau, I. Pure and Mixed Gas Acetone/nitrogen Permeation Properties of Polydimethylsiloxane [PDMS]. *J. Polym. Sci. Part B Polym. Phys.* **1998**, *36* (2), 289–301.
(89) *Physical Properties of Polymers Handbook*; Mark, J. E., Ed.; Springer New York: New York, NY, 2007.
(90) Fryer, D. S.; Peters, R. D.; Kim, E. J.; Tomaszewski, J. E.; de Pablo, J. J.; Nealey, P. F.; White, C. C.; Wu, W. Dependence of the Glass Transition Temperature of Polymer Films on Interfacial Energy and Thickness. *Macromolecules* **2001**, *34* (16), 5627–5634.
(91) Leibler, L.; Sekimoto, K. On the Sorption of Gases and Liquids in Glassy Polymers. *Macromolecules* **1993**, *26* (25), 6937–6939.
(92) Laschitsch, A.; Bouchard, C.; Habicht, J.; Schimmel, M.; Rühe, J.; Johannsmann, D. Thickness Dependence of the Solvent-Induced Glass Transition in Polymer Brushes. *Macromolecules* **1999**, *32* (4), 1244–1251.
(93) Chan, E. P.; Lee, S. C. Thickness-Dependent Swelling of Molecular Layer-by-Layer Polyamide Nanomembranes. *J. Polym. Sci. Part B Polym. Phys.* **2017**, *55* (5), 412–417.
(94) Zuo, B.; Zhang, S.; Niu, C.; Zhou, H.; Sun, S.; Wang, X. Grafting Density Dominant Glass Transition of Dry Polystyrene Brushes. *Soft Matter* **2017**, *13* (13), 2426–2436.